



The Structural and Functional Basis of Catalysis Mediated by NAD(P)H:acceptor Oxidoreductase (FerB) of *Paracoccus denitrificans*

Vojtěch Sedláček¹, Tomáš Klumpler², Jaromír Marek², Igor Kučera^{1*}

¹ Department of Biochemistry, Faculty of Science, Masaryk University, Brno, Czech Republic, ² Central European Institute of Technology, Masaryk University, Brno, Czech Republic

Abstract

FerB from *Paracoccus denitrificans* is a soluble cytoplasmic flavoprotein that accepts redox equivalents from NADH or NADPH and transfers them to various acceptors such as quinones, ferric complexes and chromate. The crystal structure and small-angle X-ray scattering measurements in solution reported here reveal a head-to-tail dimer with two flavin mononucleotide groups bound at the opposite sides of the subunit interface. The dimers tend to self-associate to a tetrameric form at higher protein concentrations. Amino acid residues important for the binding of FMN and NADH and for the catalytic activity are identified and verified by site-directed mutagenesis. In particular, we show that Glu77 anchors a conserved water molecule in close proximity to the O2 of FMN, with the probable role of facilitating flavin reduction. Hydride transfer is shown to occur from the 4-*pro-S* position of NADH to the solvent-accessible *si* side of the flavin ring. When using deuterated NADH, this process exhibits a kinetic isotope effect of about 6 just as does the NADH-dependent quinone reductase activity of FerB; the first, reductive half-reaction of flavin cofactor is thus rate-limiting. Replacing the bulky Arg95 in the vicinity of the active site with alanine substantially enhances the activity towards external flavins that obeys the standard bi-bi ping-pong reaction mechanism. The new evidence for a cryptic flavin reductase activity of FerB justifies the previous inclusion of this enzyme in the protein family of NADPH-dependent FMN reductases.

Citation: Sedláček V, Klumpler T, Marek J, Kučera I (2014) The Structural and Functional Basis of Catalysis Mediated by NAD(P)H:acceptor Oxidoreductase (FerB) of *Paracoccus denitrificans*. PLoS ONE 9(5): e96262. doi:10.1371/journal.pone.0096262

Editor: Pratul K. Agarwal, Oak Ridge National Laboratory, United States of America

Received: November 29, 2013; **Accepted:** April 5, 2014; **Published:** May 9, 2014

Copyright: © 2014 Sedláček et al. This is an open-access article distributed under the terms of the Creative Commons Attribution License, which permits unrestricted use, distribution, and reproduction in any medium, provided the original author and source are credited.

Funding: This research was supported by grants P503/10/P217 (to VS) and P503/12/0369 (to IK) from the Czech Science Foundation (www.gacr.cz) and by project Employment of Best Young Scientists for International Cooperation Empowerment, reg. number CZ.1.07/2.3.00/30.0037 co-financed by the European Social Fund and the state budget of the Czech Republic. The funders had no role in study design, data collection and analysis, decision to publish, or preparation of the manuscript.

Competing Interests: The authors have declared that no competing interests exist.

* E-mail: ikucera@chemi.muni.cz

Introduction

There is an expanding list of bacterial flavoenzymes that display redox activities against diverse xenobiotics, such as heavy metal ions like chromate [1], nitro compounds [2], azo dyes [3] and carbonyl compounds including quinones [4]. These enzymes occur as homodimers or homotetramers with a non-covalently bound flavin mononucleotide (FMN) cofactor and display a bi-bi ping-pong mechanism with NAD(P)H as the presumed physiological reductant. Despite a progress in elucidating high-resolution structures of some representatives and understanding the underlying flavin redox chemistry, key questions remain still open, in particular as regards the identity of natural substrates and the true significance in bacterial metabolism.

The flavoprotein FerB (ferric reductase B, a product of gene 4071) was originally isolated from the cytoplasm of the soil bacterium *Paracoccus denitrificans* as one of two major enzymes able to reduce Fe(III)-ligand complexes when NADH was the electron donor [5]. The protein is also active as a chromate reductase [5,6] and, to a substantially greater extent, as a quinone reductase [5,7]. Among the soluble quinone substrates tested, 2,3-dimethoxy-5-methyl-1,4-benzoquinone (ubiquinone-0, UQ-0) yielded the highest k_{cat}/K_m specificity ratio, suggesting that FerB may, in vivo, interact

with benzoquinone ring of UQ-10, a lipophilic electron carrier abundantly present in the cytoplasmic membrane of the bacterium.

An initial Pfam domain analysis [7] placed FerB within the protein family of NADPH-dependent FMN reductases (Pfam database accession number PF03358). Some members of this family contain by themselves a non-covalently bound flavin cofactor (as does FerB) and are in fact quinone reductases, catalyzing two-electron reduction of quinones to respective hydroquinones [4]. Since modulation of the intracellular activity of quinone reductases in many instances affects cell responsiveness to redox stressors, these enzymes are believed to serve as protective devices for preventing semiquinone formation and subsequent free radical production or for quinone-mediated quenching of H₂O₂ [8]. However, additional roles beyond detoxification are not excluded as well. For example, there is evidence that eukaryotic quinone reductases associate with the 20S proteasome in redox state dependent manner and control in this way proteasomal degradation of some transcription factors [9]. From the practical point of view the substrate specificity towards metal ions makes these enzymes good candidates for biodegraders of highly toxic inorganic contaminants such as chromate or uranyl [10]. They

may also find therapeutic application in prodrug processing by reductive enzymatic activation [11].

In this study, our main goal is to identify the amino acid residues of FerB responsible for flavin cofactor binding and/or catalysis of its redox conversions. For this, the crystal structure of holoenzyme has been solved and the effect of mutating the strategically selected residues has been analyzed by means of fluorimetric titration of free flavin by apoenzyme, enzyme kinetic assays and spectropotentiometry. Although there are no direct structural data on the enzyme-NADH complex, novel pieces of information about the interactions of FerB with NADH are provided by the observed stereochemistry of hydride abstraction from NADH and computer docking analyses. We also show that a simple steric modulation of the active site enhances its ability to reduce external flavin, which is otherwise negligible for the wild-type enzyme.

Materials and Methods

Gene Cloning, Protein Expression and Purification

The cloning, expression, and purification of the FerB protein and its selenomethionine derivative with a C-terminal six-histidine tag (FerBHis₆) in *E. coli* strain BL21(DE3) pLysS cells (Invitrogen) were carried out as described in the paper [12].

Site-directed Mutagenesis

Site-directed mutagenesis was carried out as specified in the QuikChange II Site-Directed Mutagenesis Kit (Stratagene). The pET21-ferB plasmid served as a PCR template; the primers are listed in Table S1. After the mutagenesis protocol, the sequences of the new *ferB* constructs were verified by sequence analysis. The mutated plasmids were purified using the Plasmid Mini DNA Purification Kit (Qiagen) and transformed into the host expression strain *E. coli* BL21(DE3) pLysS (Invitrogen). Expression of the recombinant protein mutants and the purification procedure by Ni-IDA (GE Healthcare) chromatography were performed as described for the wild-recombinant type enzyme [13]. Correct folding of all mutant enzymes was confirmed by circular dichroism spectroscopy.

Crystallization, X-ray Data Collection and Structure Determination

Crystallization, X-ray diffraction data collection and reduction of the native FerBHis₆ and its selenomethionine derivative are described in [12]. The crystal structure of FerBHis₆ protein was determined by multiple wavelength anomalous dispersion using selenium anomalous signal. Excellent data quality and resolution allow us to try to solve phase problem of FerBHis₆ using the advanced 3W-MAD protocol of Auto-Rickshaw: the EMBL-Hamburg automated crystal structure determination platform [14]. The Auto-Rickshaw structure determinative resulted in almost complete model of Se-Met FerBHis₆ homodimer containing 349 residues (out of 380) divided into 9 chains with $R/R_{free} = 0.2144/0.2682$. Detailed description of the Auto-Rickshaw strategy in this particular case is described in [15]. Missing fragments were manually built using Coot [16] and this model of FerBHis₆ was re-refined against 1.40 Å diffraction data and rebuild using PDB-REDO algorithm [17]. Final model of FerB (PDB ID: 3U7R) contains 364 residues with $R/R_{free} = 0.16065/0.17386$.

Structure Alignments

A search for sequence and structural analogy was done using Basic Logical Alignment Search Tool (BLAST) and DALI server [18]. Multiple alignment analysis and phylogenetic tree construction was done using the PHYLIP program.

SAXS (Small-angle X-ray scattering)

The SAXS data were collected on the BioSAXS-1000, Rigaku at CEITEC (Brno, Czech Republic). Data were collected at 290.15 K with X-ray beam wavelength $\lambda = 1.54$ Å. Sample to detector (PILATUS 100K, Dectris Ltd.) distance was 0.4 m covering a scattering vector range from 0.008 to 0.65 Å⁻¹. For buffer and sample one two-dimensional image was collected with an exposure time of 30 min per image. The sample was measured at three concentrations: 5.0, 2.5 and 1.25 mg/mL. The buffer was identical to the buffer of the last step of the protein purification. Data reduction and the buffer subtraction were performed using SAXSLab, Rigaku. Subtracted data were normalized to the protein concentration and truncated to 0.2 Å⁻¹. Evaluation of the solution scattering of the FerBHis₆ crystal structure and the fitting to experimental data was performed by CRYSOLO [19]. The oligomeric state of the protein was evaluated using OLIGOMER [20] where the form-factors files were created by FFMAKER using dimeric and tetrameric assembly of the FerB crystal structure, both programs from ATSAS package [21] SAXS. Data collection and scattering-derived parameters are summarized in Table S2.

Preparation of Apoflavoproteins

Approximately 2 mg of purified FerBHis₆ or its mutants in the buffer containing 50 mM sodium phosphate, 300 mM NaCl and 10 mM imidazole, pH 8.0 were applied onto a 5 mL pre-equilibrated Ni Sepharose 6 Fast Flow column (GE Healthcare). After loading the protein, the column was washed 20 mL of starting buffer. Protein-bound flavins were then removed by washing the column with 100 mL of the same buffer additionally with 4 M KBr and 4 M urea (pH 8.0). The apo-form of the protein (apoFerBHis₆) was eluted by the buffer containing 50 mM sodium phosphate, 300 mM NaCl and 500 mM imidazole, pH 8.0 (buffer C).

Analytical Size Exclusion Chromatography

0.1 mL of sample (0.5 mg/mL of proteins) was loaded onto Superose 12 (GE Healthcare) analytical and preparative column (30 cm × 1 cm) equilibrated by 25 mM Tris-HCl (pH 7.4). The flow rate after sample application was 0.5 mL/min. Marker proteins were albumin (67 kDa), ovalbumin (43 kDa), chymotrypsinogen A (25 kDa) and ribonuclease A (13.7 kDa).

DSC (Differential scanning calorimetry)

Calorimetric measurements were performed on a VP-DSC MicroCalorimeter (MicroCal) with the cell volume 0.5 mL. Data were collected from 25 to 95 °C at a heating rate of 60 °C per hour. Protein concentrations were adjusted to 2.5 mg/mL for FerBHis₆ and 4.3 mg/mL for apoFerBHis₆ in buffer C. All solutions were degassed before measurements. Reference baseline was obtained by buffer vs. buffer scan and subtracted from the measured data. The obtained data were analyzed using the Origin software (Microcal Software).

Dissociation Constants

Dissociation constants of apoenzyme-flavin complexes were determined from fluorescence titration with excitation at 450 nm by adding of constant amount of the wild-type and mutant variants of apoFerBHis₆ into 25 mM Tris-HCl buffer (pH 7.4) with 100 nM FMN or riboflavin. Decreasing emission intensities at 519 nm were recorded on Luminescence Spectrotometer LS-50B (Perkin-Elmer). Series of different concentrations of FMN standard was used for setting of a calibration curve on fluorescence

intensity. The dissociation constants K_d were calculated according to [22] and converted to the binding Gibbs energy changes $\Delta G_b = -RT \ln (1/K_d)$ (where R, gas constant, T, absolute temperature), from which the variation of Gibbs energy due to mutation ($\Delta\Delta G_b$) was computed as the difference in binding energy between mutant and wild-type enzyme ($\Delta\Delta G_b = \Delta G_b(\text{mut}) - \Delta G_b(\text{wt})$).

Steady-State Kinetics

The initial velocity of NADH oxidation was measured spectrophotometrically at 340 nm ($\epsilon = 6.22 \text{ mM}^{-1} \text{ cm}^{-1}$) after the addition of variable concentrations of NADH to the solution containing the enzyme and a fixed concentration of electron acceptor (UQ-0 or flavin) in 25 mM Tris-HCl (pH 7.4). The kinetic parameters \pm standard error were determined by fitting the data to the appropriate kinetic equation using nonlinear regression and the program Microcal Origin (version 5.0).

Determination of the Standard Redox Potential

The standard redox potentials of FerBHis₆ and its mutants were determined at 25 °C according to the method of Massey [23]. The reaction mixture contained in 1-mL cuvette the appropriate amount of the protein, 40 μM Indigo Carmine or 15 μM phenosafranin, 0.4 mM xanthine, 5 μM benzylviologen in 50 mM sodium phosphate buffer with 0.1 mM EDTA (pH 7.0). After flushing by argon (99.9999%, (v/v)), a catalytic amount of milk xanthine oxidase (0.16 μM) was added to the mixture and the reduction of FerBHis₆-bound FMN and the dye was recorded by UV-VIS spectrophotometer (UltraSpec 2000, GE Healthcare). For each time, the concentrations of oxidized and reduced FMN and dyes at 450 nm and 521 nm (phenosafranin) or 610 nm (Indigo Carmine) corrected for the contribution of the appropriate dye and FMN, were quantified.

Rapid Kinetics Measurements

Stopped-flow spectrophotometry was performed on a SFM-3000 (Bio-Logic) stopped-flow system equipped with a 0.8- \times 0.8-mm cuvette (FC-08). The temperature was kept constant at 10 °C with a thermostating water bath. Six measurements were averaged for each sample. In a typical run 75 μL of a 30 μM protein solution was mixed with 75 μL of 10 mM NADH. A flow speed of 7 ml/s resulted in a dead time of 0.4 ms. Results from the stopped-flow experiments were analyzed in the Bio-Kine software (BioLogic).

Stereospecificity Determination

[4A-²H]NADH was prepared by mixing of 5.6 mM NAD⁺, 48 mM deuterated ethanol-d₆ (99,5% D, Sigma), 25 units of horse-liver alcohol dehydrogenase, 17 units of yeast aldehyde dehydrogenase in 10 mL of 6 mM Bis-Tris/Propane Buffer (pH 9.0) at 25 °C. The pH was maintained at constant level of the buffer with additions of KOH. The end of the reduction was reached during 1-2 hours and was confirmed at 340 nm. The enzymes were removed on ice by ultrafiltration through YM3 (cut-off limit 3kDa) filters (Millipore). The temperature of the filtrate was decreased to -20 °C and [4A-²H]NADH was lyophilized by LyoQuest (Telstar). [4B-²H]NADH was prepared by mixing of 4.5 mM NAD⁺, 5 mM ATP, 6 mM deuterated D-glucose-1-d (98% D, Aldrich), 10 mM MgSO₄, 3.5 units of yeast hexokinase and 4 units of glucose-6-phosphate dehydrogenase in 10 mL of 6 mM Tris-HCl buffer (pH 8.0) at 25 °C. The removing of the enzymes and lyophilization were described above. Enzymes and nucleotides were purchased from Sigma. The specifically deuterium-labelled reduced coenzymes were reoxidized by

FerBHis₆. The total reaction volume was 1 mL of 50 mM sodium phosphate buffer (pH 7.4) and contained approximately 5 mM [4A-²H]NADH or [4B-²H]NADH, 10 mM 1,4-BQ (1,4-benzoquinone) and 5 μM enzyme. When there was no further decrease at 340 nm, the mixture was ultrafiltered and lyophilized as was described above. The lyophilized samples of NAD⁺ were dissolved in deuterium oxide (99.8%, Sigma) and all NMR spectra were measured at 25 °C on a Bruker Avance 500 MHz spectrometer (Bruker). The control spectra of 10 mM 1,4-BQ and 1,4-BQH₂ were also recorded and no interference was observed in the area of the H-4C resonance signal. Chemical shifts are expressed as p.p.m. relative to trimethylsilan.

In-silico Docking

AutoDock Vina v1.1.2 was used as a docking tool to generate putative NAD⁺/FerBHis₆ complex. Input files were prepared using the *Autodock Tools* where Gasteiger charges were assigned to a ligand and receptor and subsequently non-polar hydrogens were merged. The FerBHis₆ receptor was set as rigid during docking and the grid box with dimensions of 15 \times 15 \times 15 Å was placed into the NAD⁺ binding pocket. Exhaustiveness of the search was set to the value of 20 while all other *AutoDock Vina* parameters were kept as default. For FMN/FerBHis₆ complex generation, the FMN coordinates were removed from the FerBHis₆ receptor file. The grid box was with dimensions of 40 \times 40 \times 40 Å was placed into the FMN binding pocket, the receptor was set as rigid and all other *AutoDock Vina* parameters were kept as default.

Results

Crystal Structure of FerBHis₆

The crystal structure of FerBHis₆ in solution was determined by the multiple wavelength anomalous dispersion method using 1.40 Å resolution diffraction data (Table 1) from crystals of a selenomethionine derivative (PDB ID: 3U7R). The crystals belong to the orthorhombic space group P2₁2₁2 with two protein molecules in an asymmetric unit. The final model contains residues 2-182 (monomer A and B), one polyethylene glycol fragment, 451 water molecules and two flavin adenine mononucleotides. Most residues in the model are well defined in the 2F_o - F_c electron density map; missing density at the C terminus corresponds to the hexahistidine end (residues 184–190). The two monomers are identical with an r.m.s.d. (root mean square deviation) between equivalent C- α atoms of 0.08 Å. Each monomer has an α/β twisted open-sheet structure containing alpha helices on both sides of the central β -sheet in an arrangement typical for a flavodoxin-like fold. Five parallel strands in the order β 2, β 1, β 3, β 4, β 5, are sandwiched between the helices α 1 and α 5 on one side and the helices α 2, α 3 and α 4 on the other side. There are two ₃10 helices (residues 40–42 and 48–53) between β 2 and α 2 and a short ₃10 helix (residues 149–151) between β 5 and α 5 (Figure 1).

Quaternary Structure of FerBHis₆

The two molecules of the asymmetric unit form a head-to-tail homodimer with two symmetrical active sites facing the opposite sides and located at the interface between the subunits. Dimerization occurs mainly via anti-parallel packing of helices α 3 and α 4 into a four-helix bundle. A total of 23 residues from each monomer is involved in dimer formation (contact criteria Van der Waals overlap > -0.4 Å). The interface area of this particular assembly covers 1115.9 Å² according to a surface area analysis by PISA [24], which strongly favors it against two other possible dimeric assemblies generated in the crystal lattice (interface areas

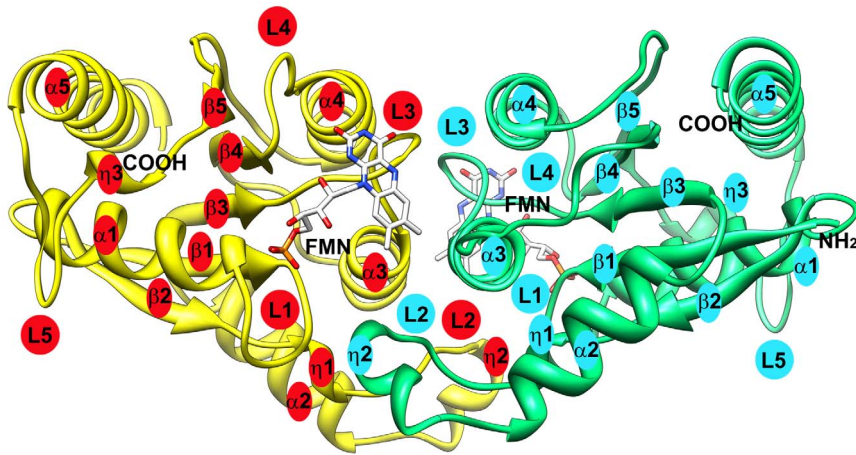


Figure 1. Overall structure of FerBHis₆ from *P. denitrificans*. The two protein subunits are shown in yellow and green ribbon representation and two bound FMN cofactors as stick models. The secondary structural elements (five α -helices, three 3_{10} helices, five β -sheets and five loops) are designated α , η , β and L and numbered as they appear along the polypeptide chain. doi:10.1371/journal.pone.0096262.g001

739.2 \AA^2 or 397.1 \AA^2). Moreover, the adjacent dimers might possibly interact through flat parts of their surfaces and pack perpendicular to one another to form a tetramer (buried area 12586.5 \AA^2).

In order to determine the actual oligomeric state of FerBHis₆ in solution, size-exclusion chromatography was first carried out on a calibrated Superose 12 column. The protein eluted at a volume of 9.5 mL (Figure S1), corresponding to 1.88 subunits with molecular mass of 21 288 Da organized in a single molecule. The prevalence of a dimeric form of FerB at moderate dilutions agrees with the results of earlier studies using chemical crosslinking or light scattering [13]. The behavior in more concentrated solutions was assessed by SAXS. The theoretical SAXS profiles of the tetramer and dimer were calculated from the crystal structure by the CRYSOLO program and compared with the experimental scattering curves obtained at protein concentration of 5, 2.5 and 1.25 mg/mL (Figure S2A). For concentrations 5 and 2.5 mg/mL, the experimental data were better fitted by the tetramer ($\chi_{5} = 1.69$ and $\chi_{2.5} = 1.27$) than the dimer ($\chi_{5} = 8.53$ and $\chi_{2.5} = 5.02$) model, while for the lowest, both fits gave nearly the same values $\chi_{1.25} = 1.22$ for the tetramer and $\chi_{1.25} = 1.50$ for the dimer. This difference indicates the occurrence of a dimer-tetramer equilibrium. Analysis of the same original data for all concentrations with the program OLIGOMER estimated the partial volume fraction of dimer:tetramer to be 9:91% ($\chi^2 = 1.18$) at protein concentration 5 mg/mL, 13:87% ($\chi^2 = 1.18$) at protein concentration 2.5 mg/mL and 34:66% ($\chi^2 = 1.60$) at protein concentration 1.25 mg/mL (Figure S2B).

Similarity to Other Proteins

A search for structurally similar proteins using the structural database comparison program DALI returned about 9 hits with Z-scores above 15. The top 11 matches belonging to the protein family PF03358 and having at least 14% sequence identity with FerB are listed in Table S3. Amino acid sequences of these matches were aligned with ClustalW and PHYLIP was used to draw the phylogenetic tree (Figure 2). FerB clustered with two recently structurally characterized proteins, the *Escherichia coli* chromate reductase ChrR [25] and the *Gluconacetobacter hansenii* chromate reductase [26], and also with the *Pseudomonas aeruginosa* FMN reductase [27]. As it is shown in Figure 2A, all the 12 representatives included in the analysis share the similar conserved

sequences thought to be involved in binding of flavin and NAD(P)H [27].

Flavin Cofactor and its Binding Site

Contrary to the initial experimental hints [5], the present X-ray crystal data show unequivocally that FMN and not FAD is a true cofactor of FerB (Figure S3). The isoalloxazine ring of FMN in enzyme crystal is bent 12.8° along the N5-N10 axis. It is uncertain at present whether the initially planar oxidized isoalloxazine adopted this conformation as a result of binding to protein or whether it was only later converted to a bent semiquinone by photoelectrons generated during data collection [28]. The FMN binding site is mainly composed of residues from the loops L1 and L3, supplemented by a few residues belonging to the adjacent subunit (Tyr46, Asp48, Arg95). The proposed interactions are summarized schematically in Figure 3. L1 carries a variant of the (T/S)ARXXS(X(T/S)) motif for phosphate binding [27], namely SLRKDSLNL, of which Ser11, Arg13, Ser16, Leu17, and Asn18 can form hydrogen bonds with the nonbridging oxygen atoms of the FMN phosphate. The amino acid residues 77 to 80 of L3 are expected to participate as follows. Glu77 and Arg80 are bonded with one another and maintain two molecules water in positions which allow to protonate the O2 atom of isoalloxazine. Alternatively, the proton for O2 can come from the hydroxyl group of Ser113. Tyr78 probably binds FMN through a stacking interaction with the dimethylbenzene end of the isoalloxazine ring; the phenolic hydroxyl group of Tyr78 could have a hydrogen bond with a phosphate oxygen atom via a molecule of water. The peptide backbone nitrogen atom of Asn79 and Arg80 can interact with N5 and O4 of isoalloxazine. As a result, FMN is anchored into the pocket in such a way that the pyrimidine end on the isoalloxazine ring remains accessible to the solvent and thus available for interacting with electron donors and acceptors.

Preparation and Characterization of Apoenzyme

The immobilized metal-affinity chromatography method of apoflavoprotein preparation, originally developed for the flavin-containing PAS domain of the NifL protein from *Azotobacter vinelandii* [29], proved to be convenient also for FerBHis₆, although the concentrations of urea and KBr had to be raised to 4 M for both in order to remove FMN most effectively. The procedure

Table 1. Data collection and refinement statistics.

Data set	3W-MAD data, Se-Met			Hi-res
	Se-peak	Inflection point	High-energy remote	Se-Met
Space group	P2 ₁ 2 ₁ 2	P2 ₁ 2 ₁ 2	P2 ₁ 2 ₁ 2	P2 ₁ 2 ₁ 2
Unit-cell Parameters (Å)	<i>a</i> = 61.22	<i>a</i> = 61.25	<i>a</i> = 61.25	<i>a</i> = 61.03
	<i>b</i> = 89.19	<i>b</i> = 89.22	<i>b</i> = 89.24	<i>b</i> = 89.14
	<i>c</i> = 71.46	<i>c</i> = 71.49	<i>c</i> = 71.53	<i>c</i> = 71.28
Wavelength (Å)	0.97714	0.97753	0.97522	1.000036
Resolution range (Å)	30–1.75 (1.78–1.75)	30–1.75 (1.78–1.75)	30–1.75 (1.78–1.75)	19.11–1.40 (1.44–1.40)
<i>R</i> _{sym} (%)	5.7 (33.7)	6.0 (41.2)	5.2 (41.7)	5.5 (28.0)
<i>I</i> / <i>σ</i> <i>I</i>	14.8 (2.2)	14.0 (1.8)	10.7 (1.4)	19.5 (3.3)
Completeness (%)	86.1 (68.0)	85.8 (66.0)	80.5 (57.7)	97.2 (86.2)
Redundancy	3.8 (1.9)	3.8 (1.9)	2.2 (1.3)	5.7 (2.2)
Wilson B factor (Å ²)	21.8	22.9	23.7	15.0
Refinement				
Resolution (Å)				19.11–1.40 (1.44–1.40)
No. Reflections				72133 (4622)
<i>R</i> _{work} / <i>R</i> _{free} (%)				16.0 (21.4)/17.4 (22.4)
No. Atoms				
Protein				2848
Ligand/ion				90
Water				451
B factor (Å²)				
Protein				9.368
Ligand/ion				11.465
Water				20.158
RMS deviations				
Bond lengths (Å)				0.013
Bond angles (°)				1.765
ESU (Å)				0.033

doi:10.1371/journal.pone.0096262.t001

yielded apoenzyme with less than 0.1% residual enzymatic activity and no appreciable absorption in the visible region. At least 99% of the original activity could be recovered upon incubation with a surplus of the native flavin. Elution volume in the gel permeation chromatography (Figure S1) of apoFerBHis₆ were similar if not identical to that of FerBHis₆, demonstrating that the apoenzyme lacking FMN still retains the ability to form a homodimer. The deflavinated product showed decreased storage stability and precipitated slowly after being transferred to low ionic strength buffers. When subjected to differential scanning calorimetry, it gave an irreversible endothermic peak at 56.5 °C, which contrasts with a significantly higher temperature of 81.2 °C for denaturation of the FMN-containing holoenzyme (Figure S4). Thus, besides its catalytic role, the flavin cofactor also displays a structural function by stabilizing the dimeric FerB protein.

Binding Affinity of Apoenzyme for Flavin

Consistently with the behavior of many other flavoproteins, binding of free FMN to apoFerBHis₆ and its mutant forms was accompanied by fluorescence quenching, which provided a means to determine the ligand dissociation constants (*K_d*). The *K_d* values for complexes of apoFerBHis₆ with FMN and with riboflavin, which lacks the 5'-phosphate group of FMN, were found to be

27 ± 2 nM and 6.58 ± 0.05 μM respectively (25 mM Tris-HCl, pH 7.4, 25 °C). A 244-fold increase in *K_d* for riboflavin indicated that interaction of apoenzyme with the FMN phosphate significantly stabilizes the complex. This conclusion could be further substantiated through mutating amino acid residues, located near the phosphate terminus of the bound FMN, to alanine. The changes in the Gibbs free energy of binding ($\Delta\Delta G_b$) upon mutation were significant for Ser11, Arg13, Ser16 and Asn18 (Figure 4), giving quantitative support to the idea that these amino acid residues constitute the binding site for phosphate. Similar mutational analysis demonstrated the importance of the tyrosine residues Tyr46 and Tyr78 and possibly also Ser113 for capturing the isoalloxazine ring of FMN.

Effect of Mutations on Kinetic Parameters for Oxidation of NADH

FerB is known to catalyze oxidation of NAD(P)H by a variety of electron acceptors. To identify residues involved in NADH recognition and catalytic activity, we determined kinetic parameters of the mutant holoenzymes in the presence of a fixed concentration of UQ-0 (0.1 mM) and variable concentrations of NADH. Mutation to alanine of Ser11, Arg13, Ser16, Asn18, Tyr46, Tyr78 and Asn79 did not impair the reaction at all,

A

```

GH-ChrR_G. han -----MTTSP LHFVTL LGS LKAS FNAAVARALPEI
ChrR_E. col -----MSEKLQVVTL LGS LKGS FNGMVARTLPKI
T1501_P. aer -----MSDDIKVLGISGS LRS GSYNSAALQEAIGL
FerB_P. den -----MVKTAVMVGS LKDK LNHKLMKVQLK
Arsh_S. fle MRLRHLSDPDSL PALDKSFAIERPALGLADAPPVRI LLLYGS LARS FSRLLAVEEAARL
Arsh_S. mel MSDDSSSHDLPAANLQQLRLPDSASLRPAPSTHRPRILILYGS LRTVYSRLLAEBAERL
WrbA_E. col -----MAKVLVLYYSMYGH IETMARAVAEGA
WrbA_P. aer -----MSSPYLLVLYYSRHGATAEMARQIARGV
YhdA_B. sub -----MNMLVINQTPRKHGRTRIAASYIAAL
EmoB_Edb BNC1 -----MTYSIVAISGSPSRNSTTAKLAEYALAH
Lot6p_S. cer -----MKVGIIMGSVRAKRVCPETAAAYVKRTIENS EELLDQKLKIQV
WrbA_S. pne -----MNKIFIYAGVRNHNHKTLEYTRKLS IISRNNDVDSF

GH-ChrR_G. han APEGIAITPLGSI GTFFPHYSQDVQ-EEGFPAPVLTMAQQIATADAVVIVTPEYNYSVPCV
ChrR_E. col APASMEVNALPSIADIPLYDADVQEEGFPATVEALAEQIRQADGVVIVTPEYNYSVPCG
T1501_P. aer VPPGMSI-ELADISGIPLYNEDVY-ALGFPPAVERFREQIRAADALLFATPEYNYSMAGV
FerB_P. den AEGRLFHLLH-IGDLPHYNDLW--ADAPESVLR LKDRIEHSDAVLAI TPEYNRSPCM
Arsh_S. fle LOFFFGAETRIFDP SDFLPDQVQS--DDHPAVKELRALSEWSEGOVWCSPERHGQITSV
Arsh_S. mel LEFFFGAEVVFDP SGLPLPDAAPV--S-HPKVQELRELSI WSEGOVWCSPERHGAMTGI
WrbA_E. col SKVDGAEVVVKRVPETMPPQLF EKAGGKTQAPVATPQELADYDAIIFGTPFRFGNMSQ
WrbA_P. aer EQG-GFEARVRTYPAVSTECEAVAPDIPAEGALYATLEDLKNACGLALGSPFRFGNMSA
YhdA_B. sub YHTDLIDLSEFVLPVNGEAEQSE---L LKVKQELKQRVTKADAI VLLSPYHSGMSGA
EmoB_Edb BNC1 VLAR-SDSQGRHHVDDLPKALLRGLDSNAKLEAVDATCNADGLIVATPEYKASYTL
Lot6p_S. cer VDLQQLALPLYEDDDELIPAQIKSVDEYADSKTRSWSRIVNALDIIVFVTPQYVNWGYPAA
WrbA_S. pne RTPFNSELEISNSDSEELPKKGI D-RQSNADDDGGV I KKELES DIIISSEVYLQNVSD

GH-ChrR_G. han LKNALDWLSRVSPQ--PLACKFV LVTASP-----MIGGARAQYHLR
ChrR_E. col LKNALDWLSRRLPDQ--PLACKFVLIQTSSM-----VIGGARCQYHLR
T1501_P. aer LKNALDWASRPPEQ--PFSCKPAILGASAG-----RFGTARAQYHLR
FerB_P. den LKNALDWATRPYQGN-SWKCKPAIVICTSP-----VIGAAALQARLK
Arsh_S. fle MKAQLDHFLP LEMAGIRPTQ CRTLAVMQVSGG SQSFNAVNTLRLLGRWMRMFTIPN QSSIA
Arsh_S. mel MKAQLDHFIPLSTGSI RPTQ CRTLAVMQVSGG SQSFNAVNQMRILGRWMRMFTIPN QSSVA
WrbA_E. col MRTFLLDQTGGLWASG-ALYKGLASVFSSTG-----TGGGQEQITITSTW
WrbA_P. aer LRYFLLDGTSSLWLTG-SLVCKPAAVFTSTAS-----LHGQETTQLSML
YhdA_B. sub LKNALDFLPSSE---QFKYKPAVLLAVAG-----GKGGINALNNMR
EmoB_Edb BNC1 LKAFLDLILPQ----FALAGKAALPLATGGS-----PAHV LALDYGLR
Lot6p_S. cer LKNALDRLY----HEWHGKPAALVVS YGGH-----GSKCNDQLQ
WrbA_S. pne TKNFIERIGG-WSHLPRLAGKRFVVTLDVAESNGSDNVSEYLRDIFSYMGGLHQVSI TN

GH-ChrR_G. han QSI VFLDAYV LNR EAMIGQVTGKVDAQT-LELSDVATREFLARQLDALAALARTLSPRA
ChrR_E. col QI VFLDAMVMNR EPMGGVIQNKVDPQT-GEVIDQGTLDHLTGQLTAFGEF IQRVKI--
T1501_P. aer QI VFLDVHPLNREVMISSAQNAFDAQG--RLDDKARELIQQQLQALQLWVRRLRG--
FerB_P. den ND LHVGTVMMSMEAYIQWHAEAYAADG--SVTDEKTAKFLQGFVDAFVDWIEKHG---
Arsh_S. fle KAFQEFDAAGRMRKSPYYDR IADVMEELVRF TALVRPHREALTD RYSERKAAGHVIDEAT
Arsh_S. mel KAFQEFDAAGRMRKSPYYDR IADVMEELVRF TALVRPHREALTD RYSERKESAABELEHRV
WrbA_E. col TTAHGMVIVPIG YAAQELFDVSVQRGGTPY GATTIAGGDGSRQPSQEELSIARYQGEY
WrbA_P. aer LPLHHGMVLVGI GYSEPALLET--RGGGTPY GASHFAGADGKRSLEDEHETLCRALGKR
YhdA_B. sub TVMRGVYANVPIPKQLVLDPVHIDVEN---ATVAENIKESI KVELVEELSMFAKAGNPV
EmoB_Edb BNC1 PVVHSMGVRRHVQSFLLVQSQFVVDGKLAVEDDVASQLNNAIDHFRLSLSSEPSRHLG
Lot6p_S. cer EVVHGLKMNVIQGVAVKIPVGTIPLP----EDIVPQLSVHNEEILQLLASC IETRNRK-
WrbA_S. pne SKKDIAEAO LMEATYKIEDVLEGGIKYKTTDYQERAYQLKLI LENYDSEHF EKMYWEKK

GH-ChrR_G. han IT-----
ChrR_E. col -----
T1501_P. aer -----
FerB_P. den -----
Arsh_S. fle DLSSIIAIPQPLPESETS
Arsh_S. mel TLKSV-----
WrbA_E. col VAGLAVK LNG-----
WrbA_P. aer LAETAGK LGS-----
YhdA_B. sub -----
EmoB_Edb BNC1 HPRPSLDATRAA-----
Lot6p_S. cer -----
WrbA_S. pne RLFEANSLEEWYVENIK
    
```

B

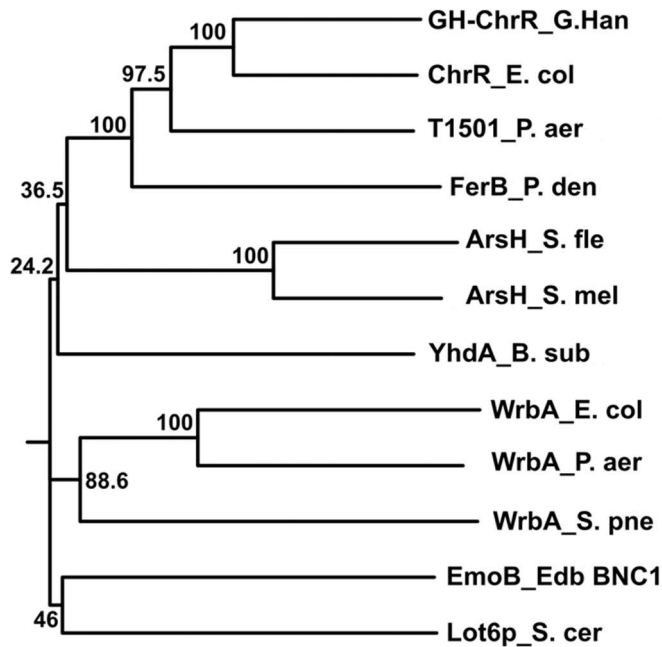


Figure 2. Tertiary structure-based sequence alignment (A) and phylogenetic tree (B) of selected structural homology proteins of FerB from a NADPH dependent FMN reductase family (PF03358). Strictly conserved residues are shown in black, dark gray shades indicate a high degree of conservation, while light grays indicate various degrees of low conservation. Generally, shaded residues indicate that a conservation of similar residues persists across at least 60% of the alignment. The alignment was generated using ClustalW with a BLOSUM62 matrix and default parameters and processed with BoxShade 3.31. Organisms and ORF designations from the corresponding genomic sequence: GH-ChrR_ *G. hanseii* (D5QFC5, gi: 388603906), ChrR_ *E. coli* (P0AGE6, gi: 84028020), T1501_ *P. aeruginosa* (Q9I4D4, gi: 81541544), FerB_ *P. denitrificans* (A1B9E3, gi: 69933457), Arsh_ *S. flexneri* (Q7UC03, gi: 75386123), Arsh_ *S. melloti* (Q92R45, gi: 81634873), WrbA_ *E. coli* (P0A8G6, gi: 67475535), WrbA_ *P. aeruginosa* (Q9I509, gi: 81622522), YhdA_ *B. subtilis* (O07529, gi: 81341002), EmoB_ Edb (EDTA-degrading bacterium) BNC1 (Q9F9T2, gi: 75466236), Lot6p_ *S. cerevisiae* (Q07923, gi: 74583672), and WrbA_ *S. pneumoniae* (Q97NR6, gi: 81531538). The phylogenetic tree with the greatest bootstrap values was constructed by a complete phylogenetic analysis package PHYLIP. doi:10.1371/journal.pone.0096262.g002

whereas mutations at residues Glu77, Arg80, Arg95, Ser113 and Gly115 were effective in decreasing k_{cat} and for most cases in increasing K_m (Table 2). The Glu77-Arg80 pair located near the

pyrimidine side of the isoalloxazine ring of FMN proved to be fundamentally important for enzyme functioning, since elimination of either member by charge-reversal or charge-neutralizing

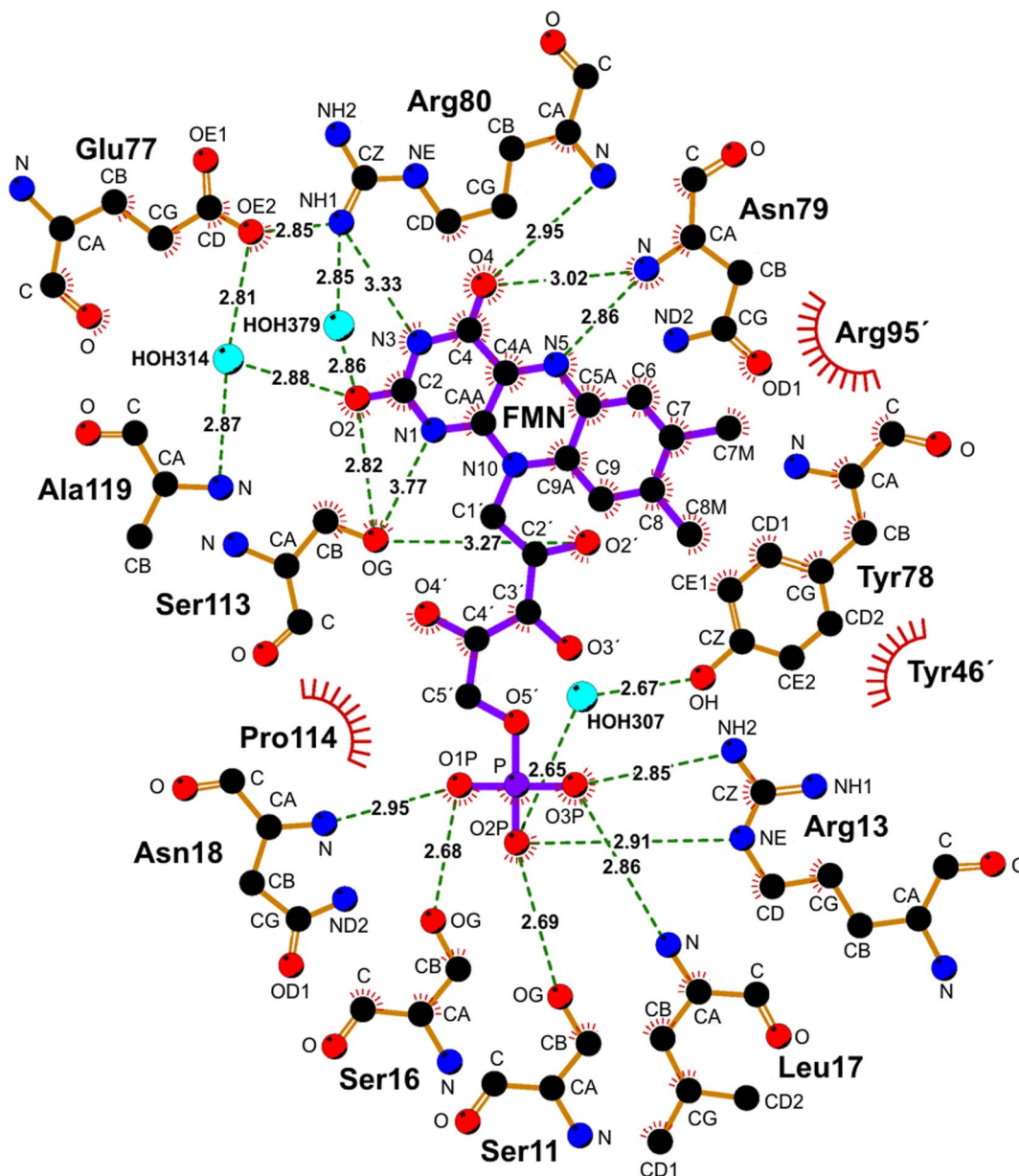


Figure 3. Predicted interactions between FMN and the protein. Hydrogen bonds are shown by dashed lines with the bond length (Å) printed in the middle, while the spoked arcs represent protein residues making nonbonded contacts with the ligand. The image was generated using the program LIGPLOT, version 4.5.3. doi:10.1371/journal.pone.0096262.g003

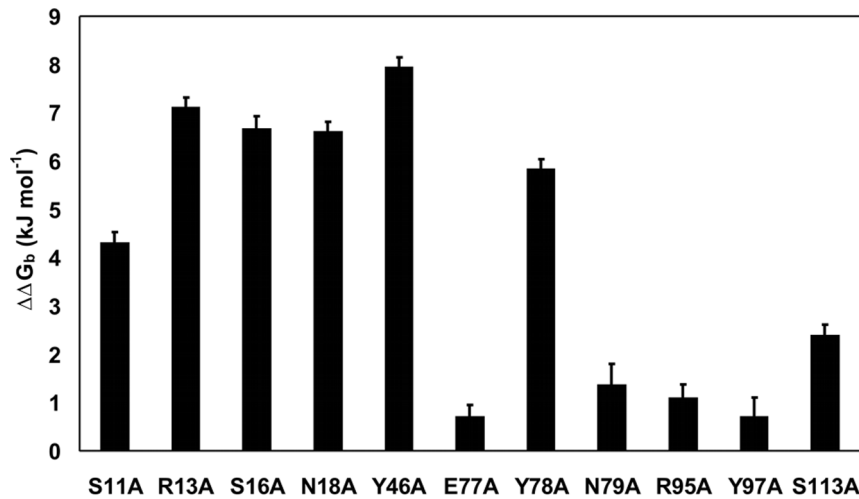


Figure 4. Changes in the standard Gibbs energy for FMN binding to alanine substitution mutants of FerBHis₆. The depicted values of $\Delta\Delta G_b$ were calculated from the dissociation constants for the mutant and wild-type protein as determined by fluorimetric titration (see Materials and Methods).
doi:10.1371/journal.pone.0096262.g004

mutation (Glu77 to Lys, Leu or Met or Arg80 to Glu, Leu or Met) reduced k_{cat} by 2 to 4 orders of magnitude. The observed changes in the apparent K_m values imply that NADH binding was mostly affected when mutations occurred at positions Arg80 and Gly115.

Flavin Cofactor Reducibility

Upon anaerobic exposure to xanthine/xanthine oxidase system at pH 7.0 the yellow flavin chromophore of FerBHis₆ was gradually reduced to its hydroquinone form without any

noticeable formation of a blue or red semiquinone radical (Figure 5A). The inclusion of indigo carmine ($E^\circ = -125$ mV, [30]) enabled us to determine the standard redox potential difference between the flavin cofactor and the reference dye (ΔE°). If a true redox equilibrium is attained, a plot of the $\log([\text{ox}]/[\text{red}])$ ratio of the enzyme versus the corresponding $\log([\text{ox}]/[\text{red}])$ ratio of the dye should produce a straight line having a slope of n_F/n_D and an intercept on the vertical axis of $-n_F\Delta E^\circ/59$, where n denotes the number of electrons needed for complete reduction of

Table 2. Kinetic parameters and standard redox potentials of FerBHis₆ for the wild-type and mutant variants.

	K_m (μM)	k_{cat} (s^{-1})	k_{cat}/K_m ($\text{mM}^{-1} \text{s}^{-1}$)	E_m (mV)	k_{obs} (s^{-1})
FerBHis ₆	22±2	258±6	11727±1100	-138±2	147.01±0.35
FerBHis ₆ -E77A	180±30	17.9±3.0	99±23	-225±10	
FerBHis ₆ -E77K	30±8	0.75 ± 0.05	25±7	-239±7	0.228±0.001
FerBHis ₆ -E77L	250±30	0.072±0.006	0.29±0.04	-229±8	
FerBHis ₆ -E77M	420±160	2.5±1.0	6.0±3.3	-223±4	
FerBHis ₆ -Y78A	40±10	196±13	4900±1267		
FerBHis ₆ -R80E	30±3	0.275 ± 0.006	9.2±0.9	-230±7	0.608±0.003
FerBHis ₆ -R80K	350±80	9.5±1.4	27±7	-148 ± 2	
FerBHis ₆ -R80M	780±280	0.302±0.084	0.39±0.18	-148±6	
FerBHis ₆ -R80L	580±150	0.142 ± 0.030	0.24±0.08		
FerBHis ₆ -R95A	20±2	146±4	7292±756	-217±11	
FerBHis ₆ -R95E	70 ± 9	21.1±0.9	302±41	-245±1	45.15±0.09
FerBHis ₆ -S113A	60±20	76.7±7.2	1278±443	-239±1	27.88±0.03
FerBHis ₆ -G115F	410±90	2.2±0.3	5.4±1.4		2.607±0.007
FerBHis ₆ -G115I	630±70	1.7±0.1	2.7±0.3	-149±3	
FerBHis ₆ -G118F	85 ± 6	77±9	906±124		
FerBHis ₆ -G118I	38±3	12±1	316±36		

The apparent Michaelis constant (K_m) for NADH and the catalytic constant (k_{cat}) were obtained by the initial velocity kinetic analysis at a constant UQ-0 concentration of 0.1 mM. The standard two-electron redox potential (E°) was determined spectrophotometrically by equilibrating the protein with a redox dye. The first-order rate constant for flavin cofactor reduction (k_{obs}) was measured upon rapid mixing the enzyme with 5 mM NADH at 10 °C under anoxic conditions. Experimental details on these measurements are given under Experimental Procedures section.
doi:10.1371/journal.pone.0096262.t002

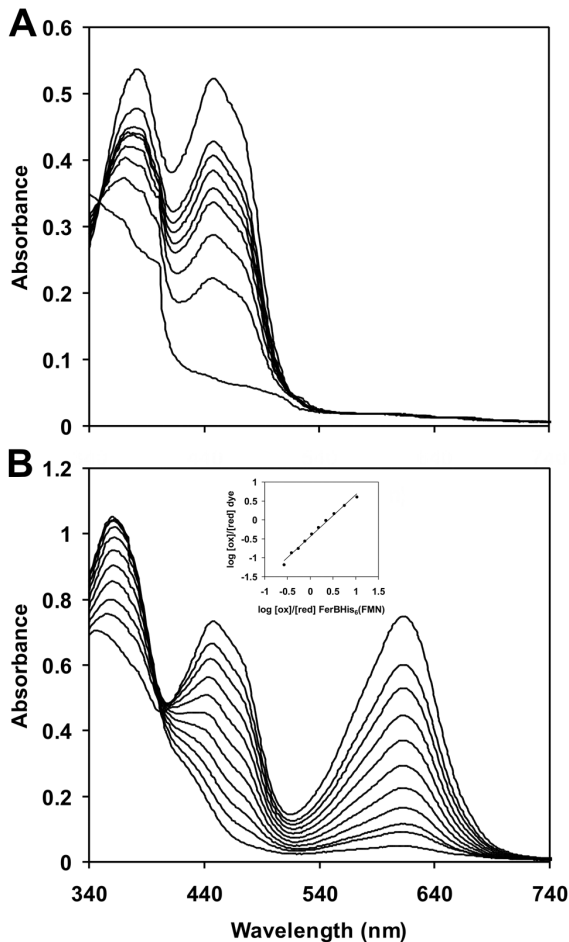


Figure 5. Spectral changes during the anaerobic reduction of FerBHis₆ by the xanthine/xanthine oxidase system. The spectra shown (from top to bottom) were recorded at 0, 5, 10, 13, 17, 22, 26, 30 and 36 min for 48 μM FerBHis₆ (A) and 0, 5, 10, 15, 20, 24, 27, 30, 33, 37 and 40 min for 65 μM FerBHis₆ with 40 μM Indigo Carmine. In (B), the inset shows the $\log(\text{ox}/\text{red})$ for the dye vs. that for the enzyme bound FMN revealing a slope of 1.08, which is close to the theoretical value of 1. The standard potential of FMN was calculated from the y-axis intercept.
doi:10.1371/journal.pone.0096262.g005

flavin (F) or dye (D). Plotting the data in this way (Figure 5B, inset) gave a slope of 1, which is close to unity as expected for $n_F = n_D = 2$. From the intercept value of -0.45 the E° of bound FMN could be calculated as $-125 + ((59/2) \times -0.45) = -138$ mV. The experiment of Figure 5 was repeated with mutant enzymes and, when appropriate, with the alternative reference dyes phenosafranin ($E^\circ = -252$ mV, [30]) or anthraquinone-2-sulfonate ($E^\circ = -225$ mV, [31]). The results are listed in the penultimate column of Table 2. Testing our system with 50 μM free FMN, we determined an E° of -212 mV which is close to the published value of -207 mV [32]. The positive shift in E° for FerBHis₆ means that the wild-type apoenzyme binds the oxidized flavin more weakly than the reduced form, which facilitates the cofactor reduction. This preference is lost in all of the tested mutants at Glu77, in the S113A mutant and also in the R80E and R95E mutants where the positively charged guanidinium group of arginine is replaced by the negative carboxyl group of glutamate.

The reduction of the FMN group by NADH, a plausible physiological donor, was evaluated spectrophotometrically in a

stopped-flow apparatus under anaerobic conditions and at 10 $^\circ\text{C}$. Changes in flavin absorbance at 450 nm upon rapid mixing of 30 μM FerBHis₆ with 1–5000 μM NADH (final concentrations) followed single exponential decay kinetics. The fitted value of k_{obs} responded hyperbolically to the NADH concentration with the half maximal effect at 6.4 ± 1.0 μM and tended toward a limit of 147.0 ± 0.4 s^{-1} that can be considered as an apparent electron-transfer rate constant for the FerB-NADH complex. The k_{obs} determined at saturating concentration of NADH (5 mM) did not depend on pH in the interval 3–9. By substituting 99% deuterium oxide for normal water in buffer of pH 6.8, a kinetic solvent isotope effect $k_{obs}(\text{H}_2\text{O})/k_{obs}(\text{D}_2\text{O})$ of 1.9 was noted. The k_{obs} at 5 mM NADH for the mutant proteins were found to be diminished in cases where the enzymatic reaction of NADH with quinone was also impaired by the mutation (Table 2). Attempts were also made to measure the oxidation of the flavin cofactor, pre-reduced with an equivalent of sodium dithionite, by 200 μM UQ-0, but the reaction of all proteins was too rapid and completed within the dead time of the stopped-flow instrument (0.4 ms).

Stereochemistry of Flavin Cofactor Reduction

Knowledge of the crystal structure of the FerB holoenzyme was enough to predict hydrogen transfer to and from the *si*-face of the bound FMN (Figure 1). However, because our attempts to grow crystals of FerB in complex with NADH or NAD⁺ had failed, we were still left uncertain as to the stereospecificity of hydrogen removal from C4 of the dihydronicotinamide moiety of NADH. Therefore, we examined the stereochemical outcome of the FerB-mediated oxidation of NADH that was stereospecifically labeled with deuterium at either the *pro-R* or *pro-S* position. Only in the former case the ¹H NMR spectrum of the NAD⁺ product contained a signal at 8.8 p.p.m (marked by arrow in Figure S5A) typical for the 4-position of nicotinamide, so we could conclude that it is the *pro-S* hydrogen that is transferred to FMN. Quantification of the kinetic isotope effects (KIEs) for the enzyme-catalyzed UQ-0 reduction (NADH, 0.15 mM; UQ-0, 100 μM ; FerBHis₆, 0.018 μM ; pH, 7.4; 30 $^\circ\text{C}$) and for the enzyme-bound flavin cofactor reduction (NADH, 1 mM; FerBHis₆, 50 μM ; pH, 7.4; 10 $^\circ\text{C}$) using the C4 monodeuterated enantiomers of NADH gave the average KIE ratios of 5.45 ± 0.21 and 6.15 ± 0.34 for [4S-²H]NADH and 1.07 ± 0.13 and 1.05 ± 0.05 for [4R-²H]NADH. The lower reactivity of the deuterated *S*-enantiomer can be taken as confirmation of the proposed stereochemistry.

FMN and NADH Docking

The laboratory-based studies on interaction of the FerB protein with FMN and NADH were complemented with an *in silico* analysis using the *AutoDock Vina* suite. Initially, in order to assess the reliability of the docking method, FMN was picked up from the holoenzyme atomic structure (PDB ID: 3U7R) and then idealized coordinates of FMN was docked back into the rigidly fixed binding site. As illustrated in Figure S6, the docked conformation of FMN with the lowest binding energy closely resembles its crystal structure, with r.m.s.d. value of 1.1 Å for 31 non-hydrogen FMN atom pairs. The calculated K_d value of 9.9 nM agrees approximately with that obtained experimentally (27 nM, see above). NADH was docked into to the crystal structure of holoenzyme where reduced form of FMN was replaced by its oxidized form to resemble the proton transfer reaction. The complex with the lowest binding energy that matches the experimentally determined stereochemistry was chosen from approximately 100 docking results. In the putative complex (Figure S7) the nicotinamide ring of NADH is stacked

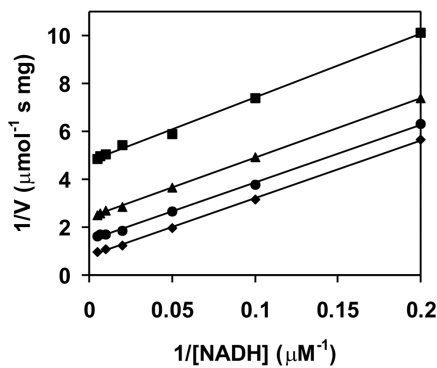


Figure 6. Initial-velocity kinetics of the NADH:FMN oxidoreductase reaction catalyzed by FerBHis₆-R95A. Measurements were performed at 30 °C with 61 nM enzyme in 25 mM Tris-HCl buffer (pH 7.4). Reciprocal initial velocity is plotted against the reciprocals of NADH concentration at a series of fixed concentrations of FMN equal to 10 (squares), 20 (triangles), 50 (circles) and 100 (rhombs) μM. doi:10.1371/journal.pone.0096262.g006

over the isoalloxazine ring of FMN with a central distance of 4.6 Å and an angle of their ring planes of 30.0°. The distance of 3.8 Å between the C4 of NADH and N5 of FMN in this complex allows the hydride transfer to occur. The residues Arg80 and Arg95 were predicted to contact the nicotinamide moiety. The carboxamide oxygen of the NADH (O7N) interacts with Arg95 (3.0 Å), while the oxygen of the ribose (O2D) interacts with Arg80 (2.9 Å). The diphosphate moiety of the NADH could interact via its O2A with the amide N of Gly115 (3.8 Å), while the adeninosine moiety interacts via O3B with Arg95 (3.2 Å) and via N6A and N7A with Arg13 (3.4 Å resp. 3.3 Å). The calculated K_d for the holoenzyme-NADH complex (4.4 μM) is consistent with the experimental K_m value for NADH (Table 2).

Engineering of the Flavin Reductase Activity

Although FerB belongs to the family of NADPH-dependent FMN reductases based on sequence homology, in fact it shows very little activity toward external FMN as compared to that toward UQ-0 as a reference, the ratio of the respective k_{cat} values being only about 0.006. A possible reason may be a steric hindrance preventing the binding of two flavins at once. Inspection of the structure suggested that removal of the bulky arginine side chain from position 95 might enlarge the active site pocket so that the accommodation of the second flavin molecule could be facilitated. In line with this expectation, we found that the k_{cat} ratio increased to 0.32 as a result of the R95A mutation. The flavin reductase activity of the novel mutant enzyme was subjected to a bisubstrate kinetic analysis (Figure 6). A double reciprocal plot of initial velocities versus concentrations of NADH as the varying substrate at four fixed levels of FMN gave a set of parallel lines indicating a ping-pong type of kinetic mechanism. By fitting the data by non-linear regression to the appropriate kinetic model, the catalytic constant and the Michaelis constants for NADH a FMN were calculated to be $50 \pm 5 \text{ s}^{-1}$, $33 \pm 7 \text{ μM}$ and $111 \pm 15 \text{ μM}$. Riboflavin and FAD were also substrates exhibiting k_{cat} values of $75 \pm 10 \text{ s}^{-1}$ and $38 \pm 1 \text{ s}^{-1}$ and K_m values of $59 \pm 12 \text{ μM}$ and $95 \pm 7 \text{ μM}$.

Since the side chain of Arg95 protrudes into active site from the neighbor subunit across the dimeric interface, more extensive changes in quaternary structure had to be considered as an alternative explanation for the effect of the mutation. However, the persistence of a dimeric state of the mutant proteins R95A and

R95E, as verified by gel permeation chromatography (Figure S1) and SAXS (data not shown), renders this possibility unlikely.

Discussion

Proteins of the flavodoxin type display a large range of FMN binding affinity. The apoproteins of typical flavodoxins bind FMN with a subnanomolar or even picomolar K_d [33], whereas the WrbA protein of *E. coli* has a K_d as high as 2 μM [34]. FerB ($K_d = 22 \text{ nM}$) thus represents an in-between case. The much weaker binding of FMN to WrbA compared with that seen for flavodoxins was attributed to alterations of critical residues located near the plane of the isoalloxazine ring of FMN and to the reduced number of hydrogen bonds with the phosphate group [35]. For the apoflavodoxin from *Anabaena* PCC 7119, pivotal binding studies by Lostao et al. [22] exploiting not only FMN but also its shortened analogues riboflavin and lumiflavin led to a dissection of the overall Gibbs binding energy of FMN (-55 kJ mol^{-1}) into three components related to the phosphate (-29 kJ mol^{-1}), isoalloxazine (-21 kJ mol^{-1}), and ribityl (-5 kJ mol^{-1}) parts of the molecule. An analogous calculation with the experimental K_d values for FMN (22 nM) and riboflavin (6.6 μM) shows that only $-13.6 \text{ kJ mol}^{-1}$ of the total $-43.2 \text{ kJ mol}^{-1}$ apparently comes from the phosphate, i.e., that the relative importance of isoalloxazine may be higher for FerB than for the *Anabaena* flavodoxin. In most flavodoxins isoalloxazine is sandwiched between the aromatic residues tyrosine and tryptophan at the *si*-face and *re*-face, respectively [36]. In FerB only the *re*-face residue remains aromatic (Tyr78) and, as indicated by mutant analysis, adds to the binding, the contribution of the *si*-face arginine (Arg95) being negligible. Yet another tyrosine residue (Tyr46), which extends from the second subunit and has its phenolic ring positioned nearly perpendicularly, appears to interact with the flavin at its dimethylbenzene end by providing a hydrophobic environment. The binding of the flavin ring is further strengthened by hydrogen bonds with Ser113 and two backbone NH groups (not quantifiable by alanine mutagenesis). Alanine substitutions were also helpful in confirming the presumed role of Ser11, Arg13, Ser16 and Asn18 in binding the phosphate moiety. The sum of $\Delta\Delta G_b$ values of the individual mutations equals 24.7 kJ mol^{-1} , which greatly exceeds the value of 13.6 kJ mol^{-1} expected from the FMN and riboflavin binding data. We interpret this discrepancy to mean that the $\Delta\Delta G_b$ values cannot be simply added because there are some cooperative interactions among the spatially close residues.

Detailed structural studies of NADH binding to FerB-like enzymes are generally hampered due to the lack of co-crystals suitable for X-ray diffraction. At present, the only available data are those of the NADH:FMN oxidoreductase (EmoB) from *Mesorhizobium* sp. BNC1 [37] that has 21% sequence identity with FerB. In the crystal structure of the EmoB-FMN, NADH complex (PDB ID: 2VZJ), the *si*-face (B-side) of the nicotinamide ring of the pyridine nucleotide packs against the *si*-face of the isoalloxazine ring of FMN, as is likely to be the case for FerB. The amine group of Lys81 and the backbone carbonyl group of Gly112 in EmoB were considered to bind to the carboxamide and phosphate groups of NADH, respectively [37]. According to the results of amino acid sequence comparison (Figure 2A), the amino acid at position 81 is not conserved and EmoB is the only member that has a lysine at this site. The equivalent residue in FerB, Asn79, was mutated to Ala without affecting enzyme activity. On the contrary, Gly112 of EmoB is strictly conserved among all the sequences. The corresponding Gly115 in FerB is located on a turn between strand β4 and helix α4 within a sequence motif SXGXXG that is

reminiscent of the common GXGXXG fingerprint region of the classical Rossmann fold. These glycine-rich regions are typically involved in positioning dinucleotides in a correct conformation by allowing for close contact of the polypeptide chain with its central diphosphate portion [38]. Our finding that introduction of a large phenylalanine or isoleucine substitution at amino acid 115 results in a one-order increase in K_m for NADH and two-order decrease in k_{cat} (Table 2) is consistent with (but does not in itself prove) the idea of Gly115 being a part of the NADH binding site. In our model of the FerB-NADH docked complex, Gly115 lies indeed within hydrogen-binding distance of a O2-phosphate oxygen of NADH and clear steric hindrances occurs following superimposition of Phe or Ile on it. The same Phe or Ile substitutions at the more distant Gly-118 were much less effective. Arg80 may also participate in NADH binding, since its substitutions strongly affected the K_m value. In this case the docking model predicts interaction with the hydroxyl group of NADH ribose.

New structural data link FerB very closely to the recently characterized chromate reductases (ChrR) of *Escherichia coli* (PDB ID: 3SVL) and *Gluconacetobacter hansenii* (PDB ID: 3S2Y). One thus would expect that all three enzymes might operate by the same overall mechanism, but this need not necessarily be true. Previously it was claimed that the reduction of chromate by NADH catalyzed by *G. hansenii* ChrR proceeds via an ordered, sequential reaction with chromate binding first followed by NADH and that binding of NADH alone produces a death-end complex [26]. Some facts about FerB, however, contradict this picture. When catalyzing a reaction of between NADH and quinone, FerB obeys a ping-pong type reaction mechanism [5], which is consistent with a temporary parking of reducing equivalents from NADH at the enzyme-bound flavin cofactor. Prestationary assays reported here show that the flavin group of FerB is still reducible by NADH despite the absence of any electron acceptor like quinone or chromate. The estimated limiting k_{obs} ($\sim 140 \text{ s}^{-1}$ at 10°C) is similar to the steady-state value of k_{cat} for the NADH-driven reduction of UQ-0. Taking also into account a comparable deuterium kinetic isotope effect upon both processes, we conclude that (i) an electron-acceptor-independent reduction of flavin is operative, (ii) it is kinetically competent to account for the observed enzyme activity, and (iii) it may be rate-limiting for the whole catalytic cycle, at least with UQ-0 as electron acceptor.

Following hydride transfer to the N5 position of the flavin, stabilization of the negative charge evolving at the N1-C2=O2 locus of the isoalloxazine moiety is required. In flavoenzymes this is usually accomplished through the interaction with a positively charged entity, either fully charged, such as a Lys or Arg side chain, or partially charged, such as the N terminus of a helix or a cluster of peptide nitrogen [39]. In the canonical crystal structure of the rat liver quinone reductase (PDB ID: 1QRD) O2 of the FAD cofactor is hydrogen-bound to the backbone amide groups of Gly149 and Gly150 and also to the side chain of Tyr155. It was postulated that Tyr155 and the neighboring His161 form a charge-relay system needed for the reaction to take place without unfavorable charge separation [40]. FerB and the ChrR proteins of *E. coli* and *G. hansenii* are distinguished by a different microenvironment of the N1-C2=O2 locus, comprising a hydroxyl group of serine and a water molecule hold in position by a glutamate-arginine pair. The residues Ser113 and Glu77 of FerB are well conserved among the homologous sequences (Figure 2A). The importance of Ser113 gains support from experiments of the alanine mutant that exhibits lower specific activity as well as depressed FMN binding. The involvement of water in catalysis by FerB is consistent with the observed solvent

isotope effect of 1.9 for FMN reduction, suggesting that an oxygen-hydrogen bond is broken in a rate limiting step. Water has already been proposed to serve as a proton donor to N1 or O2 atoms at flavin reduction in several other flavoenzymes, such as NADPH-cytochrome P450 oxidoreductase (PDB ID: 1AMO; [41]), 2,4-dienoyl-CoA reductase (PDB ID: 1PS9; [42]), FMN-dependent azoreductase (PDB ID: 2HPV; [43]) and peptidyl-cysteine decarboxylase (PDB ID: 1G5Q; [44]). A crucial role of Glu77, amply substantiated by the results of mutational experiments, probably relates to maintaining the architecture of the active site. Unlike FerB, where a pair Glu77-Arg80 exists, the homologous glutamate in both of the ChrR enzymes pairs with a more remote arginine located 43 amino acid residues away. In *E. coli* ChrR this arginine lies at the surface and participates in dimer-dimer interaction [25]. Subtle differences in hydrogen bond networks in ChrR and FerB thus may explain why the former enzyme forms a stable homotetramer while the latter remains dimeric in dilute solutions.

Of the proteins similar to FerB listed in Table S3, five have been demonstrated to catalytically reduce flavin, i.e., to act as an NADH:flavin oxidoreductase. Judging from their crystal structures, these enzymes have the flavin cofactor largely exposed to the bulk solvent, whereas in FerB the dimethylbenzene part of the flavin nucleus appears to be shielded by the side chain of the Arg95 residue from the neighbor protomer within the homodimeric structure. The mutant protein R95A, prepared from FerB_{His6} to relieve the presumed steric constraint, indeed gained the ability to reduce FMN with a k_{cat} of 50 s^{-1} , which is close to the value for the *B. subtilis* YhdA ($60\text{--}70 \text{ s}^{-1}$, [45]) but lower than that for EmoB of *Mesorhizobium* sp. bacterium BNC1 (397 s^{-1} , calculated from the V_{max} of $1111 \mu\text{mol min}^{-1} \text{ mg}^{-1}$ given in [37], using a subunit molecular mass of 21 412 Da). Similarly to EmoB, the engineered FerB obeyed a ping-pong kinetic mechanism with NADH and FMN as substrates (Figure 6) suggesting that NADH and a loosely associated FMN molecule interact in an alternating fashion with the same pocket containing another, tightly bound FMN. Such a mechanism was previously identified for EmoB through preparation and structural analysis of its FMN-NADH and FMN-FMN complexes [37]. Since a single mutation increasing the accessibility of the bound FMN sufficed for FerB to become an active flavin reductase with affinities for FMN, FAD and riboflavin (indicated by K_m values) comparable each other, isoalloxazine rings contacts may be of importance in recognition of the external flavins. According to the ^1H NMR chemical shift measurements, FMN self-associates in aqueous solutions with an association constant in the range $20\text{--}100 \text{ M}^{-1}$ [46]. This would give an expected dissociation constant of the order of 10 mM, which is however still two orders of magnitude above the estimated Michaelis constants ($\sim 0.1 \text{ mM}$). Pre-existing protein environment around the bound flavin cofactor thus probably also contributes to the external flavin substrate binding. A close relationship of FerB to the flavin reductases, demonstrated now both structurally and biochemically, may shed some light on the evolution of flavin reduction and various promiscuous catalytic activities of flavoproteins in general.

Supporting Information

Table S1 The mutagenic oligonucleotide primers for site-directed mutagenesis of FerB His₆.
(DOC)

Table S2 Data collection from SAXS.
(DOC)

Table S3 Amino-acid identity and structural similarity across the structural homologs of FerB in a FMN reductase protein family (PF03358). (DOCX)

Figure S1 Superose 12 analytical size exclusion chromatography of FerBHis₆ holoenzyme (1), apoenzyme (2), and FerBHis₆-R95E mutant (3). The calibration curve used to estimate the native molecular weight based on the elution position is indicated. (TIF)

Figure S2 SAXS scattering curves. X-ray scattering of FerBHis₆ was compared with calculated scattering of the dimer (*dashed line*) and the tetramer (*solid line*) computed by CRY SOL for concentrations 1.25 (A), 2.5 (B) and 5.0 (C) mg/mL. The program OLIGOMER was used to estimate dimer and tetramer volume fractions for concentrations 1.25 (D), 2.5 (E) and 5.0 (F) mg/ml. (TIF)

Figure S3 Electron density map of FMN. Stereo view of the $2F_o - F_c$ electron density map contoured at 1.0 σ cut-off corresponding to FMN at the active site. (TIF)

Figure S4 Thermal stability of apoFerBHis₆ (A) and FerBHis₆ (B) followed by DSC. Protein concentrations were adjusted to 4.3 mg/mL for apoFerBHis₆ and 2.5 mg/mL for FerBHis₆ in buffer C and data were collected from 25 to 95 °C at a heating rate of 60 °C per hour. (TIF)

Figure S5 NMR spectra of NAD⁺. The ¹H NMR aromatic region of NAD⁺ formed from [4B-²H]NADH (A) or [4A-²H]NADH by FerBHis₆ in the presence of 1,4-benzoquinone showing a resonance signal at 8.8-8.9 p.p.m. (A) or no resonance

signal (B). The enzyme removed the proton from B-side (pro-S, *si*-face) of the dihydrogenicotinamide ring. (TIF)

Figure S6 Superimposition of FMN from the crystal structure of FerBHis₆ (white) and from the docking-derived complex (yellow). (TIF)

Figure S7 Structure of the docked FerBHis₆-NADH complex. NADH was modeled into the FerBHis₆ structure using *AutoDock Vina v1.1.2*. FMN and NADH are shown with yellow and white carbons, respectively (A). The nicotinamide ring was stacked on top of the isoalloxazine ring at distance 3.8 Å that corresponding with distances of other NADH-dependent FMN reductases. The residues are depicted in green and violet to represent belonging to two different subunits. The known crystal structure of EmoB complex with NADH (PDB ID: 2VZJ) is included for sake of comparison (B). (TIF)

Acknowledgments

We thank to Josef Houser for calorimetric measurements on a VP-DSC MicroCalorimeter and Zbyněk Prokop and Jiří Damborský for providing access to the stopped-flow apparatus. We wish thank EMBL/DESY Hamburg for providing us with synchrotron facilities and D. Tucker for his assistance with data collection on beamlines X12 and X13 of the DORIS-III storage ring at DESY Hamburg.

Author Contributions

Conceived and designed the experiments: IK. Performed the experiments: VS TK. Analyzed the data: VS TK JM IK. Wrote the paper: IK.

References

- Ramirez-Diaz MI, Diaz-Perez C, Vargas E, Riveros-Rosas H, Campos-Garcia J, et al. (2008) Mechanisms of bacterial resistance to chromium compounds. *Biometals* 21: 321–332.
- Symons ZC, Bruce NC (2006) Bacterial pathways for degradation of nitroaromatics. *Nat Prod Rep* 23: 845–850.
- Ryan A, Laurieri N, Westwood I, Wang CJ, Lowe E, et al. (2010) A novel mechanism for azoreduction. *J Mol Biol* 400: 24–37.
- Deller S, Macheroux P, Sollner S (2008) Flavin-dependent quinone reductases. *Cell Mol Life Sci* 65: 141–160.
- Mazoch J, Tesarik R, Sedlacek V, Kucera I, Turanek J (2004) Isolation and biochemical characterization of two soluble iron(III) reductases from *Paracoccus denitrificans*. *Eur J Biochem* 271: 553–562.
- Sedlacek V, Kucera I (2010) Chromate reductase activity of the *Paracoccus denitrificans* ferric reductase B (FerB) protein and its physiological relevance. *Arch Microbiol* 192: 919–926.
- Sedlacek V, van Spanning RJ, Kucera I (2009) Characterization of the quinone reductase activity of the ferric reductase B protein from *Paracoccus denitrificans*. *Arch Biochem Biophys* 483: 29–36.
- Gonzalez CF, Ackerley DF, Lynch SV, Matin A (2005) ChrR, a soluble quinone reductase of *Pseudomonas putida* that defends against H₂O₂. *J Biol Chem* 280: 22590–22595.
- Sollner S, Macheroux P (2009) New roles of flavoproteins in molecular cell biology: an unexpected role for quinone reductases as regulators of proteasomal degradation. *FEBS J* 276: 4313–4324.
- Barak Y, Ackerley DF, Dodge CJ, Banwari L, Alex C, et al. (2006) Analysis of novel soluble chromate and uranyl reductases and generation of an improved enzyme by directed evolution. *Appl Environ Microbiol* 72: 7074–7082.
- Thorne SH, Barak Y, Liang W, Bachmann MH, Rao J, et al. (2009) CNOB/ChrR6, a new prodrug enzyme cancer chemotherapy. *Mol Cancer Ther* 8: 333–341.
- Klumpler T, Sedlacek V, Marek J, Wimmerova M, Kucera I (2010) Crystallization and initial X-ray diffraction studies of the flavoenzyme NAD(P)H:(acceptor) oxidoreductase (FerB) from the soil bacterium *Paracoccus denitrificans*. *Acta Crystallogr Sect F Struct Biol Cryst Commun* 66: 431–434.
- Tesarik R, Sedlacek V, Plockova J, Wimmerova M, Turanek J, et al. (2009) Heterologous expression and molecular characterization of the NAD(P)H:acceptor oxidoreductase (FerB) of *Paracoccus denitrificans*. *Protein Expr Purif* 68: 233–238.
- Panjikar S, Parthasarathy V, Lamzin VS, Weiss MS, Tucker PA (2005) Auto-rickshaw: an automated crystal structure determination platform as an efficient tool for the validation of an X-ray diffraction experiment. *Acta Crystallogr D Biol Crystallogr* 61: 449–457.
- Klumpler T, Marek J, Sedlacek V, Kucera I (2010) Solving phase problem using a Se-Met derivative of the flavoenzyme NAD(P)H:acceptor oxidoreductase (FerB). *Materials Structure in Chemistry, Biology, Physics and Technology* 17: b21–b23.
- Emsley P, Cowtan K (2004) Coot: model-building tools for molecular graphics. *Acta Crystallogr D Biol Crystallogr* 60: 2126–2132.
- Joosten RP, Joosten K, Murshudov GN, Perrakis A (2012) PDB_REDO: constructive validation, more than just looking for errors. *Acta Crystallogr D Biol Crystallogr* 68: 484–496.
- Holm L, Rosenstrom P (2010) Dali server: conservation mapping in 3D. *Nucleic Acids Res* 38: W545–549.
- Svergun D, Barberato C, Koch MHJ (1995) CRY SOL - A program to evaluate x-ray solution scattering of biological macromolecules from atomic coordinates. *J Appl Crystallogr* 28: 768–773.
- Konarev PV, Volkov VV, Sokolova AV, Koch MHJ, Svergun DI (2003) PRIMUS: a Windows PC-based system for small-angle scattering data analysis. *J Appl Crystallogr* 36: 1277–1282.
- Petoukhov MV, Franke D, Shkumatov AV, Tria G, Kikhney AG, et al. (2012) New developments in the ATSAS program package for small-angle scattering data analysis. *J Appl Crystallogr* 45: 342–350.
- Lostao A, El Harrou M, Daoudi F, Romero A, Parody-Morreale A, et al. (2000) Dissecting the energetics of the apoflavodoxin-FMN complex. *J Biol Chem* 275: 9518–9526.
- Massey V (1990) A simple method for the determination of redox potentials. In: Curti B, Ronchi S, Zanetti G, editors. *Flavins and Flavoproteins*. Berlin: de Gruyter W. pp. 59–66.
- Krissinel E, Henrick K (2007) Inference of macromolecular assemblies from crystalline state. *J Mol Biol* 372: 774–797.
- Eswaramoorthy S, Poulain S, Hienerwadel R, Bremond N, Sylvester MD, et al. (2012) Crystal structure of ChrR—a quinone reductase with the capacity to reduce chromate. *PLoS one* 7: e36017.
- Jin H, Zhang Y, Buchko GW, Varnum SM, Robinson H, et al. (2012) Structure determination and functional analysis of a chromate reductase from *Gluconacetobacter hansenii*. *PLoS one* 7: e42432.

27. Agarwal R, Bonanno JB, Burley SK, Swaminathan S (2006) Structure determination of an FMN reductase from *Pseudomonas aeruginosa* PA01 using sulfur anomalous signal. *Acta Crystallogr D Biol Crystallogr* 62: 383–391.
28. Rohr AK, Hersleth HP, Andersson KK (2010) Tracking flavin conformations in protein crystal structures with Raman spectroscopy and QM/MM calculations. *Angew Chem Int Ed Engl* 49: 2324–2327.
29. Hefü MH, Milder FJ, Boeren S, Vervoort J, van Berkel WJ (2003) A His-tag based immobilization method for the preparation and reconstitution of apoflavoproteins. *Biochim Biophys Acta* 1619: 139–143.
30. Tedeschi G, Chen S, Massey V (1995) DT-diaphorase. Redox potential, steady-state, and rapid reaction studies. *J Biol Chem* 270: 1198–1204.
31. Tedeschi G, Zetta L, Negri A, Mortarino M, Cecilian F, et al. (1997) Redox potentials and quinone reductase activity of L-aspartate oxidase from *Escherichia coli*. *Biochemistry* 36: 16221–16230.
32. Mayhew SG (1999) Potentiometric measurement of oxidation-reduction potentials. *Methods Mol Biol* 131: 49–59.
33. Bollen YJ, Westphal AH, Lindhoud S, van Berkel WJ, van Mierlo CP (2012) Distant residues mediate picomolar binding affinity of a protein cofactor. *Nat Commun* 3: 1010.
34. Grandori R, Khalifah P, Boice JA, Fairman R, Giovanielli K, et al. (1998) Biochemical characterization of WrbA, founding member of a new family of multimeric flavodoxin-like proteins. *J Biol Chem* 273: 20960–20966.
35. Ji HF, Shen L, Carey J, Grandori R, Zhang HY (2006) Why WrbA is weaker than flavodoxin in binding FMN. A molecular modeling study. *Theochem-J Mol Struct* 764: 155–160.
36. Sancho J (2006) Flavodoxins: sequence, folding, binding, function and beyond. *Cell Mol Life Sci* 63: 855–864.
37. Nissen MS, Youn B, Knowles BD, Ballinger JW, Jun SY, et al. (2008) Crystal structures of NADH:FMN oxidoreductase (EmoB) at different stages of catalysis. *J Biol Chem* 283: 28710–28720.
38. Bellamacina CR (1996) The nicotinamide dinucleotide binding motif: A comparison of nucleotide binding proteins. *Faseb J* 10: 1257–1269.
39. Fraaije MW, Mattevi A (2000) Flavoenzymes: diverse catalysts with recurrent features. *Trends Biochem Sci* 25: 126–132.
40. Li R, Bianchet MA, Talalay P, Amzel LM (1995) The three-dimensional structure of NAD(P)H:quinone reductase, a flavoprotein involved in cancer chemoprotection and chemotherapy: mechanism of the two-electron reduction. *Proc Natl Acad Sci U S A* 92: 8846–8850.
41. Hubbard PA, Shen AL, Paschke R, Kasper CB, Kim JJ (2001) NADPH-cytochrome P450 oxidoreductase. Structural basis for hydride and electron transfer. *J Biol Chem* 276: 29163–29170.
42. Hubbard PA, Liang X, Schulz H, Kim JJ (2003) The crystal structure and reaction mechanism of *Escherichia coli* 2,4-dienoyl-CoA reductase. *J Biol Chem* 278: 37553–37560.
43. Liu ZJ, Chen HZ, Shaw N, Hopper SL, Chen LR, et al. (2007) Crystal structure of an aerobic FMN-dependent azoreductase (AzoA) from *Enterococcus faecalis*. *Arch Biochem Biophys* 463: 68–77.
44. Blaesse M, Kupke T, Huber R, Steinbacher S (2000) Crystal structure of the peptidyl-cysteine decarboxylase EpiD complexed with a pentapeptide substrate. *Embo J* 19: 6299–6310.
45. Deller S, Sollner S, Trenker-El-Toukhy R, Jelcsarov I, Gubitzi GM, et al. (2006) Characterization of a thermostable NADPH:FMN oxidoreductase from the mesophilic bacterium *Bacillus subtilis*. *Biochemistry* 45: 7083–7091.
46. Bastian M, Sigel H (1997) The self-association of flavin mononucleotide (FMN(2-)) as determined by ¹H NMR shift measurements. *Biophys Chem* 67: 27–34.